Double Gyroid Morphologies in Precise Ion-Containing Multiblock Copolymers Synthesized via Step-Growth Polymerization

Jinseok Park[a] and Karen I. Winey[a,b,*]

[a]Department of Materials Science and Engineering
University of Pennsylvania, Philadelphia, Pennsylvania 19104, United States
[b]Department of Chemical and Biomolecular Engineering
University of Pennsylvania, Philadelphia, Pennsylvania 19104, United States

Abstract

The double gyroid structure was first reported in diblock copolymers about 30 years ago and the complexity of this morphology relative to the other ordered morphologies in block copolymers continues to fascinate the soft matter community. The double gyroid microphase-separated morphology has co-continuous domains of both species and the minority phase is subdivided into two interpenetrating network structures. In addition to diblock copolymers, this structure has been reported in similar systems including diblock copolymers blended with one or two homopolymers and ABA-type triblock copolymers. Given the narrow composition region over which the double gyroid structure is typically observed (~ 3 vol%), anionic polymerization has dominated the synthesis of block copolymers to control their composition and molecular weight. This perspective will highlight recent studies that (1) employ an alternative polymerization method to make block copolymers and (2) report double gyroid structures with lattice parameters below 10 nm. Specifically, step-growth polymerization linked precise polyethylene blocks and short sulfonate-containing blocks to form strictly alternating multiblock copolymers and these copolymers produce the double gyroid structure over a dramatically wider composition range (> 14 vol%). These new $(AB)_n$ multiblock copolymers self-assemble into the double gyroid structure by having exceptional control over the polymer architecture and large interaction parameters between the blocks. This perspective proposes criteria for a broader and synthetically more accessible range of polymers that self-assemble into double gyroids and other ordered structures, so that these remarkable structures can be employed to solve a variety of technological challenges.

Keywords: double-gyroid, self-assembly, ion-containing polymers, multiblock copolymers, block copolymers

Double Gyroid Morphologies in Block Copolymers

The double gyroid (DG) structure is a 3-dimensionally periodic bicontinuous structure with $Ia\bar{3}d$ symmetry that consists of two interpenetrating networks of the minority component and a matrix of the majority component (**Figure 1**). This ordered structure with $Ia\bar{3}d$ symmetry was first identified in strontium lipids in 1967.[1] The first report of the DG structure in block copolymers was made in 1994.[2] Since then the DG has intrigued the polymer science community due to its structural complexity compared to the more common ordered structures of layers and hexagonally-packed cylinders found in linear block copolymers.[2] Moreover, the percolating domains of the DG morphology contribute to enhancing mechanical properties such as modulus, toughness, and creep resistance of materials relative to the other morphologies.[3–5] The bicontinuous domains of DG can also improve ionic conductivities when the interpenetrating domains contain ionic functionalities.[6–9] The triply periodic structure of DG can even control the optical properties and its application into metamaterials.[10–13]

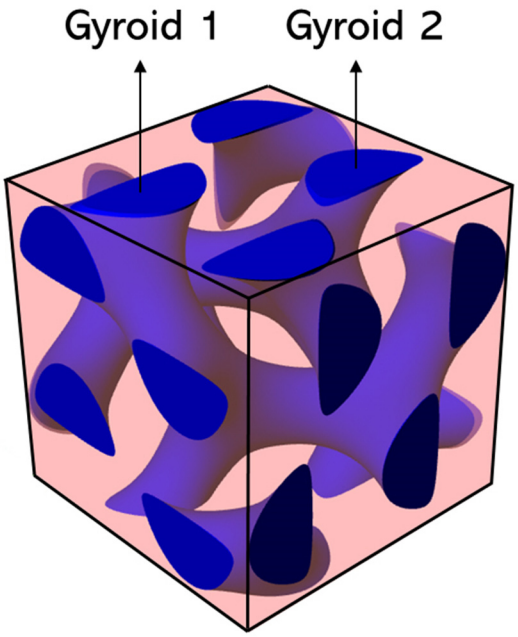

Figure 1. The cubic unit cell of a double-gyroid morphology with $Ia\bar{3}d$ symmetry, showing the two interpenetrating networks of the minority component (blue) with a volume fraction of 0.30.

Followed by the first assignment of DG in the linear polystyrene-polyisoprene diblock copolymers (PS-*b*-PI),[2] comprehensive investigations of polystyrene-polyisoprene block copolymers have advanced the understanding of the structural characteristics of DG in polymeric systems.[14–18] Note that the DG structures in star block copolymers and other block copolymer systems were originally reported to be double-diamond morphologies with *Pn3m* symmetry and were later correctly identified as exhibiting the DG.[18] Subsequently, various block chemistries including polystyrene-*b*-poly(2-vinyl pyridine),[19,20] polyethylene-*b*-polyethylethylene,[21,22] and many others[23,24] also identified the DG in diblock copolymers. Building upon the design rules to generate DG structures from linear diblock copolymers, self-consistent field theory (SCFT) was utilized to predict the equilibrium morphologies within the χN-*f* phase diagram, where χ, *N*, and *f* are the Flory-Huggins interaction parameter, degree of polymerization, and the volume fraction of one block component, respectively. The SCFT revealed that the DG structure is thermodynamically stable within a relatively narrow volume fraction range of ~3.7 vol% at intermediate segregation strength of χN = 20 and ~1.5 vol% at strong segregation of χN = 100 (**Figure 2a**).[25] Note that the DG was originally found to be unstable at high-χN values due to the increased sharpness at the interface and packing frustration, while experiments and recent SCFT calculations find that the DG exists at high χN.[25–28]

The narrow composition range of DG in conventional linear diblock copolymers is due to the triply periodic minimal surface and chain packing within the DG. Specifically, polymer chains should minimize the interfacial area and uniformly fill the domains defined for each block species.[29,30] Linear diblock copolymers that satisfy both conditions are often limited to only a few volume fraction range according to the self-consistent field theory (SCFT) calculation. Experimentally, PS-*b*-PI diblock copolymers self-assemble into the DG structures at f_{PI} = 0.36 – 0.39 and 0.65 – 0.68 (**Figure 2b**).[17,31] The DG structures have been widely observed in more complicated polymer systems than simple diblock copolymers, such as AB/A diblock copolymer/homopolymer blends,[2,32,33] AB/A`B` binary diblock copolymer blends,[21,34] tapered block copolymers,[35] and ABA triblock copolymers.[4,36–38] In addition, ABC triblock copolymers exhibit a core-shell type DG ($Ia\bar{3}d$ symmetry)[39–42] and alternating gyroid ($I4_132$ symmetry)[43–45] structures depending on the block species. DG structures exist at a wider volume fraction range in

diblock/homopolymer, due to the additional chain ends and increased chain length dispersity that alleviates packing frustration.[46–48] For example, polystyrene-*b*-polyisoprene diblock copolymers (10.1 kg/mol PS and 17.3 kg/mol PI) with homopolystyrene (760 g/mol hPS) or homopolyisoprene (650 g/mol hPI) blends demonstrated that the volume fraction window for the DG structure increases up to ~12 vol% after a long time of annealing (**Figure 2c**).[2] Alternatively, introducing a more flexible linkage between blocks of diblock copolymers expands the accessible DG window (**Figure 2d**).[49] A comprehensive phase map of PI-*b*-PS-*b*-PEO identified core-shell DG structures with PS encapsulating PEO to form both gyroid structures when the PI matrix volume fraction was 0.45 – 0.50.[40–42] Note that these block copolymers have been synthesized using predominantly anionic polymerization methods to control the composition range required to produce the DG with a molecular weight dispersity index of 1.01 - 1.11.[20,24,50] While the polydispersity index can significantly impact the self-assembly of block copolymers,[51–54] dissipative particle dynamics simulations showed that increasing polydispersity index of ABA linear block copolymers results in the destabilization of ordered DG structure into disordered bicontinuous morphology.[55] Experimental studies on ABA triblock copolymers identified the disordered bicontinuous morphologies at a composition window of ~10 vol%.[56,57] In contrast, the layered morphologies of ABC triblock copolymers can transform into core-shell DG structures upon increasing the polydispersity of one block species.[58] In summary, the DG morphology has been found in a wide variety of systems containing AB, ABA, and ABC block copolymers and the composition window within which the DG morphology resides is narrowest for diblock copolymers and broadens for more complex systems.

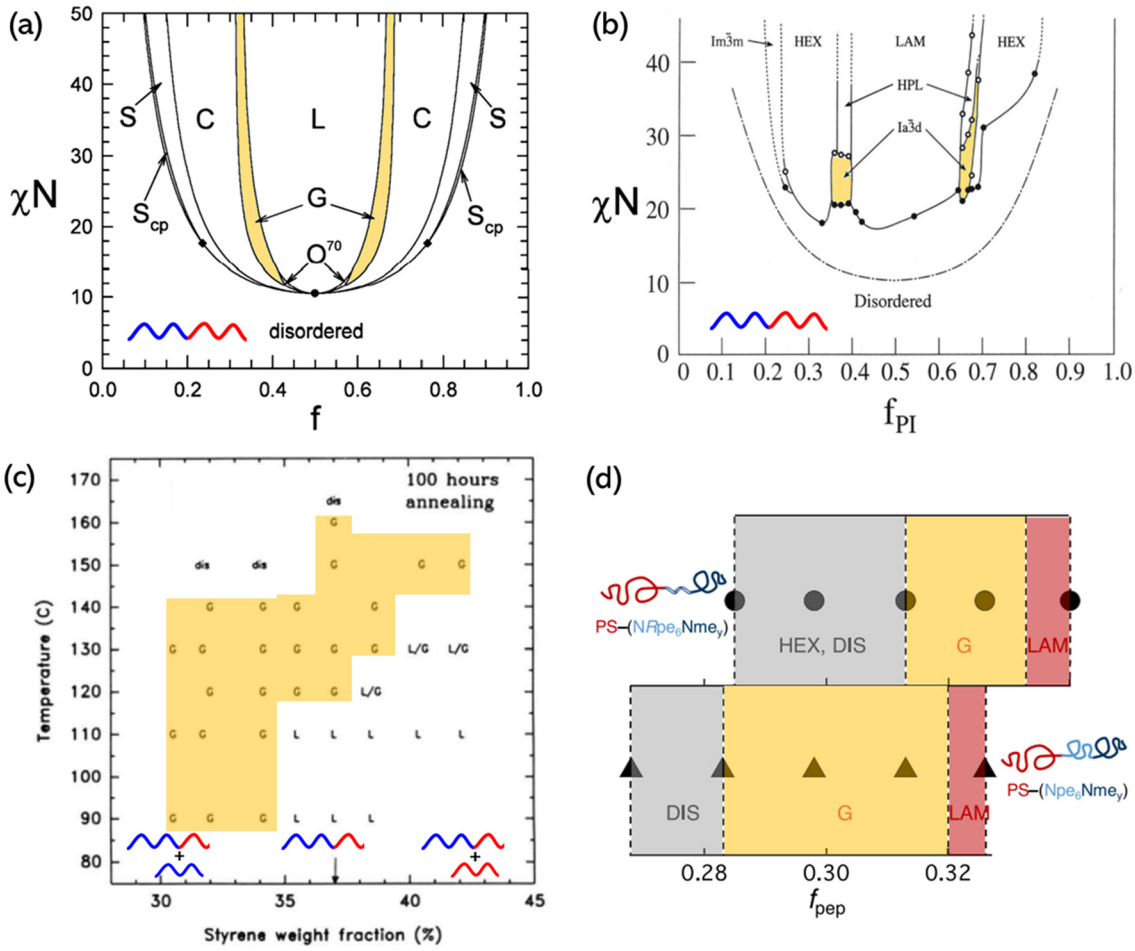

Figure 2. (a) Phase diagram for AB diblock copolymers calculated from self-consistent field theory. Adapted from ref 31. Copyright 2012 American Chemical Society. (b) Experimental phase diagram for PS-*b*-PI diblock copolymers. Adapted from ref 17. Copyright 1995 American Chemical Society. (c) Experimental phase diagram of binary blends containing a diblock copolymer (PS-b-PI) and a homopolymer (hPI or hPS). The styrene weight fraction of the pure PS-b-PI diblock copolymer is 37% (arrow). Below and above this point are blends with hPI and hPS, respectively. The shaded region indicates the range of DG morphologies. Adapted from ref 2. Copyright 1994 American Chemical Society. (d) Phase diagram of PS-polypeptoid diblock copolymers with stiff (top) and flexible (bottom) interfacial linkages. Reprinted from ref 49. Copyright 2021 American Chemical Society.

Double Gyroid Morphologies in Alternating Multiblock Copolymers

Linear $(AB)_n$ alternating multiblock copolymers have the potential for designing ordered nanostructures as they can self-assemble into various nanostructures.[59] For example, SCFT calculations predict that the equilibrium morphologies of $(AB)_n$ multiblock copolymers are identical to the conventional diblock copolymer morphologies with layers, DG, cylinders, and spheres.[31] The number of repeating units

(n) impacts various characteristics of $(AB)_n$ alternating multiblock copolymers. First, the microphase separation of multiblocks requires ~50% higher segregation strength ($\chi N_{crit} \sim 15.1$ at $n > 20$) than the diblock copolymers ($\chi N_{crit} \sim 10.5$ at $n = 1$).[60] Also, the domain spacings of ordered structures of $(AB)_n$ alternating multiblock copolymers decrease with an increasing n, particularly at $n < 10$.[61,62] Therefore, theory predicts that $(AB)_n$ multiblock copolymers at sufficiently high segregation strength will produce ordered structures, as well as the desired DG structures. Nevertheless, experimental studies showing ordered structures in linear $(AB)_n$ multiblock copolymers are far fewer as compared to studies of AB diblock copolymers, presumably due to the (1) synthetic challenges to produce alternating and monodisperse blocks and (2) insufficient block segregation strength upon increasing the number of repeating blocks. Producing $(AB)_n$ alternating multiblocks using anionic polymerization requires $2n$ polymerization steps and the polydispersity of each block length impedes the ordering of microphase separated structures. In linear (PS-*b*-PI)$_n$ multiblock copolymers, an increase of n resulted in the decrease of the grain size of the layers, *i.e.* less ordering with increasing n.[63,64] For these reasons relative to diblock copolymers, accessing ordered morphologies including the DG in linear $(AB)_n$ multiblock copolymers has been quite limited.

Recent studies of precise ion-containing copolymers highlight the phase behavior and formation of DG structures in alternating multiblock architectures. **Figure 3a** presents the step-growth synthesis of polyester sulfonate multiblock copolymers (PES*x*M) using a sulfosuccinate diester with a counterion and an alkyl diol of fixed length of x-carbons. These PES*x*M polymers are linear $(AB)_n$ multiblock copolymers with strictly alternating polar ionic and non-polar blocks. The polydispersity index for the length of AB repeating subunit (N) is exactly 1.00, because the polar and non-polar block lengths are fixed by the monomers. Note that we define N as the number of backbone atoms in the AB repeat unit, $N = x + 6$. In these $(AB)_n$ multiblock copolymers, the number of AB repeating units (n) becomes trivial with increasing n as the chain-end effects become negligible. In PES23Li the hydrocarbon blocks crystallize below the melting temperature (T_m) ~ 123 °C and the short polar blocks self-assemble into a layered (LAY) morphology as indicated by the differential scanning calorimetry (DSC) traces (**Figure 3b**). Upon heating

above the T_m, X-ray scattering with reflections peaks at √6, √8, √14, √16, √20, √22, √24, and √26 indicate that PES23Li (n = 11) forms a well-defined DG morphology at 150 °C (**Figure 3C**).[7] These peak locations unambiguously indicate the DG structure of the $Ia\bar{3}d$ space group with a cubic lattice parameter of 7.6 nm. This DG further transitions upon heating into the hexagonally packed cylinder (HEX) morphology with an order-to-order transition temperature (T_{OOT}) ~ 176 °C. Upon cooling at 1 °C/min, the phase transitions are reversible at T_{OOT} ~ 168 °C and the DG to LAY crystallization transition (T_c) at ~90°C, **Figure 3b**.

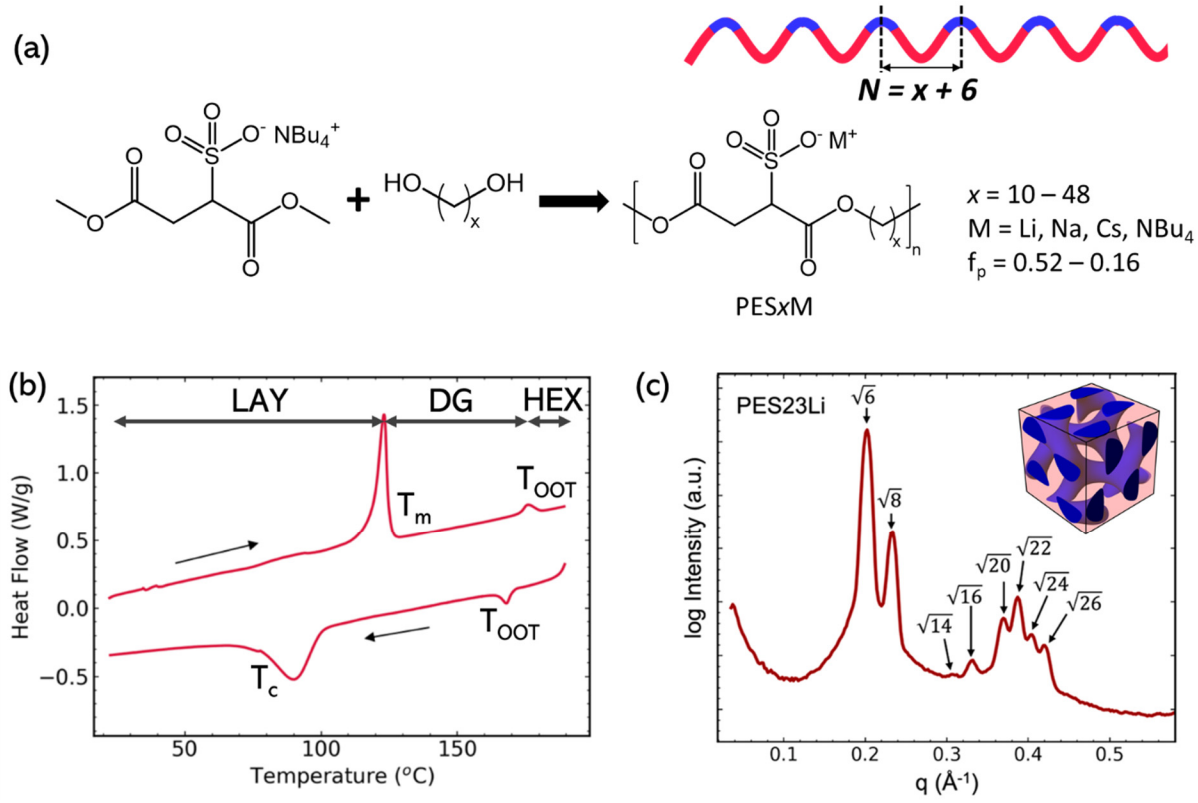

Figure 3. (a) Precise ion-containing multiblock copolymers synthesized by polycondensation of a diol and a sulfosuccinate ester, and then ion-exchange. (b) The DSC traces of PES23Li from the second heating and cooling at a ramp rate of 1 °C/min. (c) X-ray scattering of PES23Li at 150 °C identifies the double gyroid morphology ($Ia\bar{3}d$ symmetry) with a lattice parameter of 7.6 nm. (b) and (c) are adapted from ref 7. Copyright 2020 American Chemical Society.

The phase transitions found in PES23Li are altered by the choice of counterion. **Figure 4** illustrates the ionic aggregate and hydrocarbon chain structures of PES23M as a function of temperature and cation species (M = Li^+, Na^+, Cs^+, and NBu_4). $PES23NBu_4$ is an intermediate product that includes bulky

quaternary ammonium cations prior to the cation exchange with Li, Na, and Cs. For all PES23M polymers, the hydrocarbon blocks form hexagonally packed crystals below the T_m. For PES23NBu$_4$ with a bulky quaternary ammonium cation and weak electrostatic interaction, the melting transition is relatively low, T_m ~32 °C, and the polymer transitions directly from layered to disordered ionic aggregates upon heating. In contrast, PES*x*M polymers with metal cations show melting transition temperatures higher than 100 °C and produce DG structures above the T_m. The order-to-order transition temperatures (T_{OOT}) as measured by DSC increase with the increase of cation size (Li < Na < Cs). PES23Li and PES23Na show GYR – HEX transitions upon heating, while the HEX morphology is inaccessible in PES23Cs below 210 °C. When polar ionic diblocks strongly interact via Coulombic cohesion, OOT phase boundaries shift to lower values of χN.[65] Since $\chi \sim 1/T$, this implies that the T_{OOT} increases with increased Coulombic interaction between ionically charged blocks. For PES23M, the GYR to HEX T_{OOT} increases from Li to Na to Cs, indicating stronger electrostatic cohesion with increasing cation size.

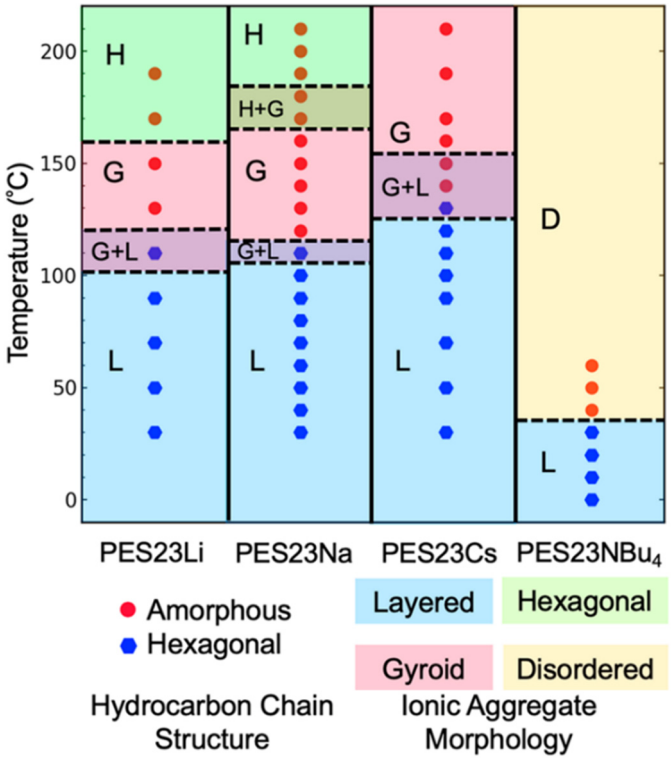

	Cation size (Å)	T_m (°C) (LAY – GYR)	T_{OOT} (°C) (GYR-HEX)
PES23Li	0.76	123	176
PES23Na	1.02	127	194
PES23Cs	1.67	139	> 210

Figure 4. Morphology summary of PES23M with varying counterion species (M = Li, Na, Cs, and NBu_4) as a function of temperature. Hydrocarbon chain structure (symbol) and ionic aggregate morphologies (shading) were determined from the *in-situ* X-ray scattering upon heating. The table summarizes the melting temperature (T_m) and order-to-order transition temperature (T_{OOT}) as determined by differential scanning calorimetry traces. The cation size is the effective radius of ions coordinated with six oxygens. Adapted from ref 7. Copyright 2020 American Chemical Society.

Effect of Volume Fraction on the Phase Behavior of PESxM

The volume fraction of the polar block in these $(AB)_n$ alternating multiblock copolymers is readily controlled by the selection of the alkyl chain length of *x*-carbons. **Figure 5** shows the temperature-dependent phase diagram of PES*x*Na (x = 48 – 10) as a function of polar volume fraction (f_p = 0.16 – 0.45) and highlights the effect of hydrocarbon chain lengths on the phase behavior.[66] In all polymers, layered

ionic aggregates coexist with a crystalline hydrocarbon block, and the T_m increases with alkyl block length: PES10Na at T_m = 91.7 °C and PES48Na at T_m = 140 °C. The increase of T_m with x indicates that longer hydrocarbon blocks crystallize into large crystals with fewer defects. Upon heating above T_m, DG morphologies are accessible at an unexpectedly wide range of volume fractions of at least 14 vol% ($0.27 < f_p < 0.41$) for PES23Na, PES18Na, and PES12Na (**Figure 5a**). This result demonstrates greater accessibility to the DG in $(AB)_n$ multiblock copolymers. These DG morphologies transition into HEX morphologies upon further heating. In contrast, LAY morphologies of PES48Na and PES10Na directly transition into the HEX morphology above the T_m. For DG-forming PES*x*Na polymers (x = 23, 18, 12), HEX – DG transitions are reversible and rapid (a few minutes) upon cooling, whereas the DG morphologies slowly crystallize into layered ionic aggregates upon further cooling below T_m (**Figure 5b**). The slow crystallization kinetics are associated with the restricted chain mobility imposed by the strong ionic interactions. In PES12Na with a short 12-carbons block, DG morphologies persist during the *in situ* X-ray scattering experiments with an average cooling rate of ~0.3 °C/min, and then gradually crystallizes at room temperature into a layered ionic aggregate morphology in about a week. Therefore, we observe kinetically trapped DG morphologies with amorphous hydrocarbon blocks upon cooling below T_m.

This kinetic competition between the self-assembly of the polar blocks and the crystallization of the hydrocarbon blocks is also evident by comparing PES48Na and PES10Na upon cooling below T_m. For PES48Na, the 48-carbon alkyl block crystallizes to form layered ionic aggregates during the *in situ* X-ray experiment, while the 10-carbon alkyl block of PES10Na persists in the HEX morphology without crystallization. Since f_p of PES48Na and PES10Na are 0.16 and 0.45, respectively, PES48Na exhibits a stronger driving force to crystallization than PES10Na. The hysteresis displayed in **Figure 5** for PES*x*Na multiblock copolymers suggests that the accessible temperature window for DG morphologies can be extended to lower temperatures, perhaps even room temperature, by impeding the crystallization of the hydrocarbon backbones. For example, substituting the linear diol with a non-crystallizable diol may produce the DG at room temperature.

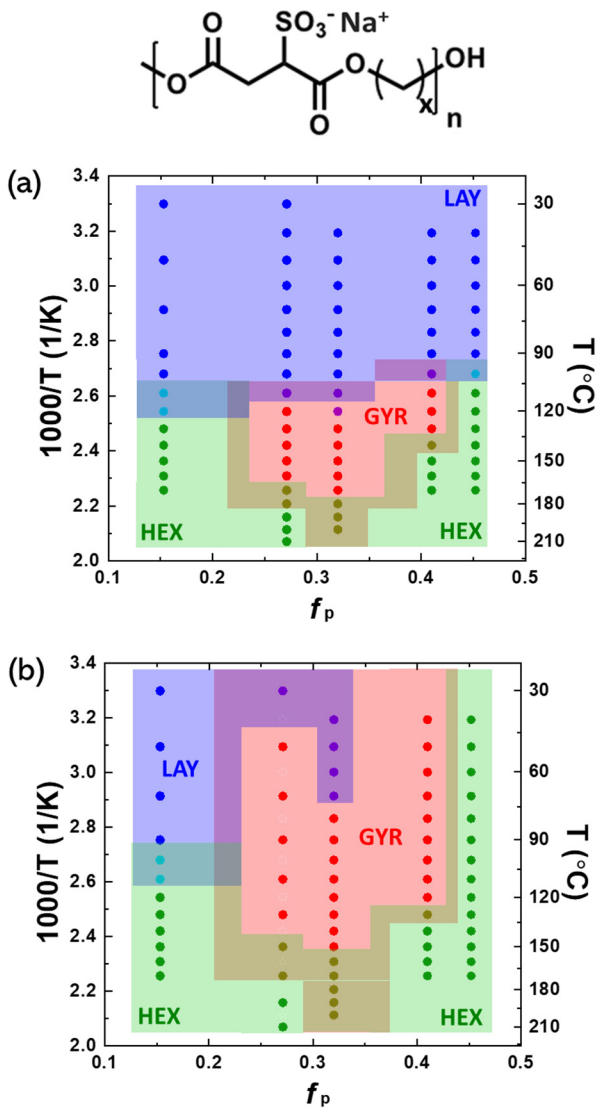

Figure 5. Morphology diagram of PES*x*Na plotted as *1/T* versus f_p while (a) heating and (b) cooling during in situ X-ray scattering experiments. The values of *x* (48, 23, 18, 12, and 10) correspond with increasing f_p. LAY (blue), GYR (red), and HEX (green) indicate layered, double-gyroid, and hexagonal ionic aggregate morphologies. Mixed phases near the transition temperatures are indicated by light blue (LAY + HEX), purple (LAY + GYR), and olive (GYR + HEX) colors. Reprinted from ref 66. Copyright 2021 American Chemical Society.

In the PES*x*Na alternating multiblock copolymers the DG structures are observed over an unexpectedly wide composition range. One explanation might be the strong electrostatic cohesion between the polar ionic blocks, which lead to asymmetric phase diagrams. In block copolymers with charged moieties tethered to the backbone, the composition of the charged block disproportionally impacts the

microphase-separated morphologies.[67–69] The physical properties of PES*x*Na, such as the non-Gaussian chain statistics of the short alternating blocks and conformational asymmetry of blocks, may further skew the phase diagram. While PES*x*M systems have charges covalently tethered to the backbone, extensive research on diblock copolymers (e.g., PS-*b*-PEO) with added salt have found that the salt content significantly impacts the equilibrium morphologies.[70–75] Specifically, a substantial shift of the phase boundaries of salt-doped block copolymers is often explained by factors including ion solvation energy and ion-ion correlations. Clearly, the thermodynamics of equilibrium morphologies in ion-containing block copolymer systems are not yet fully understood. To the best of our knowledge, theoretical studies are lacking to describe the wide range of DG structures and the phase behavior of these ion-containing $(AB)_n$ multiblock copolymers.

Figure 6 shows the isothermal lattice parameters (a) of the three ordered morphologies observed in PES*x*Na polymers along with their scaling relationships to the number of backbone atoms ($N = x + 6$). The lattice parameters are small (< 10 nm) and exceptionally well-controlled by selecting the length of the aliphatic diol monomers. The effect of n on the lattice parameter appears to be negligible for the PES*x*Na polymers, because the value of n spans from ~10 for PES23Na to ~37 for PES12Na. The SCFT for $(AB)_n$ multiblock copolymers predicts the domain spacings of layers when $n = 10$ is only slightly larger (< 2%) than that of $n = 37$. The scaling relationship of $a \sim N^{0.92}$ for LAY is attributed to the crystallization of hydrocarbon, and therefore the distance between the layered ionic aggregates is proportional to the number of carbons in the hydrocarbon block. The relationships for DG ($a \sim N^{0.67}$) and HEX ($a \sim N^{0.52}$) morphologies with amorphous hydrocarbon chains coincide with the scaling relationship of strongly and weakly segregated neutral diblock copolymers, respectively. By comparison, experimental results for diblock copolymers observed exponents of ~0.8 – 1.0.[76–79] The a-N relationships and morphology map of PES*x*Na reveal that the nanoscale ordered structures and their length scales in PESxNa multiblock copolymers can be finely tuned at the length scale of 2 - 8 nm.

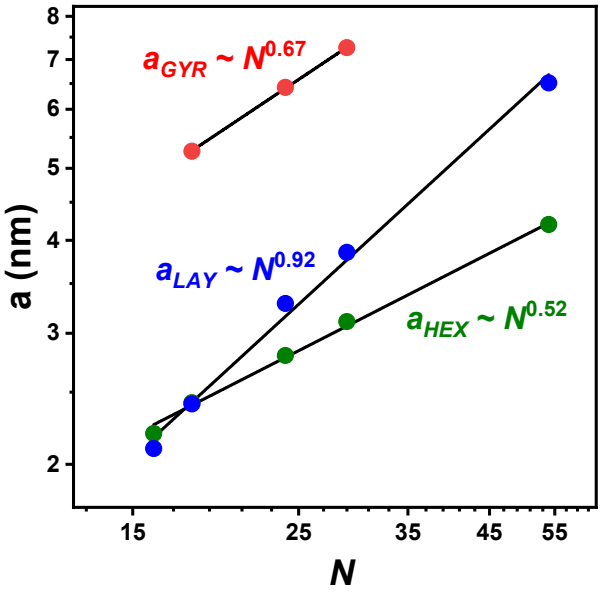

Figure 6. Lattice parameters of LAY at 40 °C (blue), DG at 130 °C (red), and HEX at 170 °C (green) morphologies for PES*x*Na polymers (x = 10 – 48). The value of N is defined as x + 6 for PES*x*Na.

Figure 7 shows the morphology diagram of PES*x*Li (x = 12, 18, 23) as a function of temperature upon heating.[62] Both PES23Li and PES18Li form DG above the T_m similar to PES23Na and PES18Na, while PES12Li exhibits disordered morphologies above T_m. Consistent with the discussion about the cation effect on the T_{OOT} for PES23M (**Figure 4**), the T_{OOT} of DG – HEX transition for PES18Li is 9.2 °C lower than PES18Na as determined from DSC. Notably, PES12Li transitions into a disordered morphology at T_m, whereas PES12Na transitions into the ordered morphologies of DG and HEX above T_m. While cation effects shown in **Figure 4** were limited to fixed x = 23, the more comprehensive effect of f_p presented in **Figure 5a** and **Figure 7** highlights the cation effects on the phase boundaries in both f_p and $1/T$.

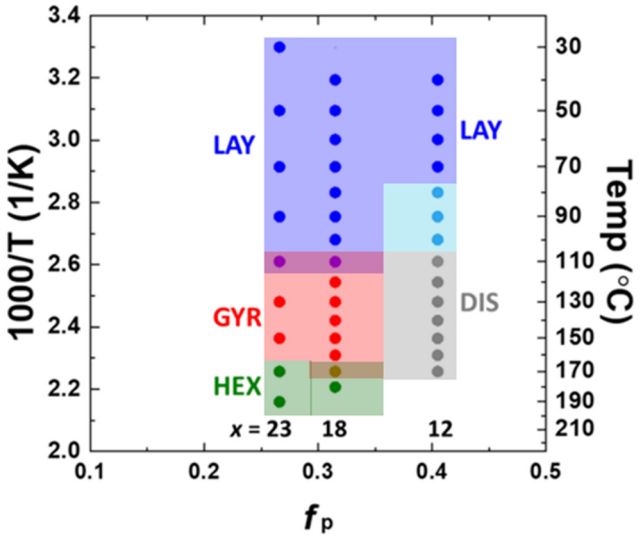

Figure 7. Morphology diagram of PES*x*Li plotted as *1/T* versus f_p upon heating during in situ X-ray scattering experiments. The colors correspond to morphology type as detailed in **Figure 5** with the addition of the disordered morphology (DIS, gray). Adapted from ref 62. Copyright 2021 American Chemical Society.

Determination of Ultrahigh-χ and χN-f Phase Diagram in PESxLi

Further development of $(AB)_n$ multiblock copolymer thermodynamics requires knowledge of block interactions. The Flory-Huggins interaction parameter (χ) is obtained from the disordered morphology of PES12Li using the random phase approximation for $(AB)_n$ multiblock copolymers (**Figure 8a**).[62] The quality of the fit of the random phase approximation theory to the experimental scattering data is high even though the alternating block lengths in PES12Li are short. In **Figure 8b**, the temperature dependence of $\chi = 77.4/T + 2.95$ (T in Kelvin) with a reference volume of 0.118 nm^3 indicates a high enthalpic contribution from ionic interactions and a high entropic contribution from short block lengths. The value of χ at 25 °C is 3.21, identifying the PES*x*Li ion-containing multiblock copolymers as ultrahigh-χ and low-N block copolymers. This is consistent with the formation of ordered nanostructures with sub-3 nm domain spacings. For comparison, the value of χ at 25 °C for polystyrene-*b*-poly(methyl methacrylate) is 0.043.[80,81] Although the χ value was inaccessible for PES*x*Na, the presence of ordered morphologies at $T > T_m$ for PES12Na and PES10Na suggests χ values even higher than PES*x*Li. The ultrahigh-χ and ordered morphologies with sub-3 nm domain spacings suggest a new direction for template-assisted nanofabrication technologies using

$(AB)_n$ multiblock copolymers.

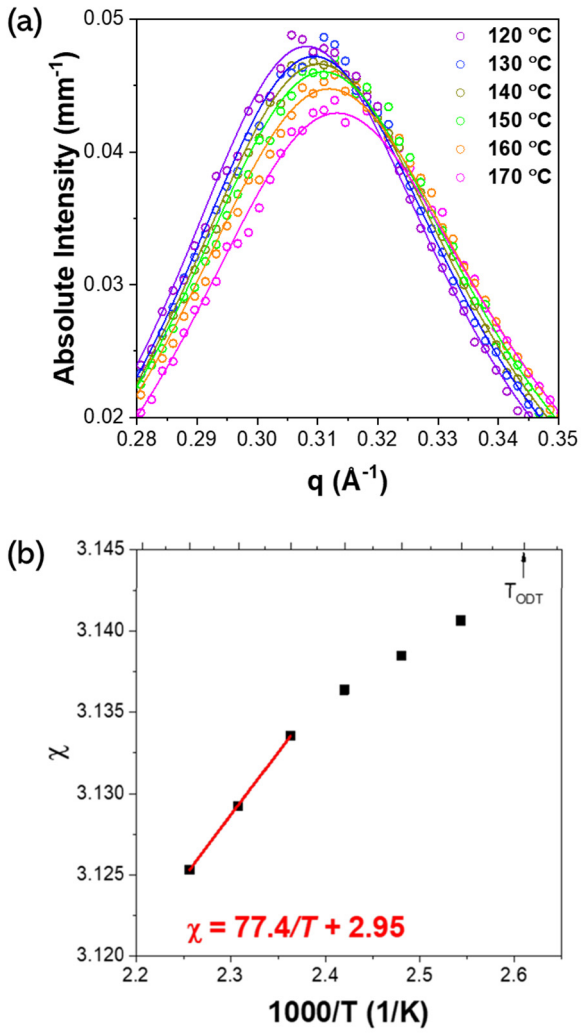

Figure 8. (a) Experimentally obtained scattering intensity (dots) of PES12Li in 10 °C increments from 120 to 170 °C. Theoretically defined scattering intensities (line) from disordered $(AB)_n$ multiblock copolymers are used to determine χ. (b) Temperature dependence of χ and the linear relationship with $1/T$ above the mean-field temperature. Reprinted from ref 62. Copyright 2021 American Chemical Society.

Figure 9 compares the experimentally observed phase transitions of PES*x*Li polymers and the phase boundaries determined from self-consistent field theory (SCFT) for $(AB)_{17}$ multiblock copolymers. The experimentally observed morphology transitions of PES*x*Li polymers are offset from the SCFT predictions: GYR−HEX transitions for PES23Li and PES18Li, and LAY−DIS transition for PES12Li are shifted to a lower f_p relative to the theoretical boundaries. The discrepancies between the phase behavior of PES*x*Li and the SCFT phase boundaries can be attributed to the short block lengths and the electrostatic

interactions between the polar blocks. Theoretically, mean-field approximations including the self-consistent field theory (SCFT) used to describe the uncharged polymer systems are insufficient for predicting phase behavior in electrostatically charged systems because of the field fluctuations.[82–84] Theoretical models have introduced the fluctuation effects to consider the electrostatic interactions in the phase-separated polymer systems.[82–84] More recently, a polarizable field-theoretic model explored the electrostatically stabilized microphase separation in a blend of oppositely charged polymer systems, which showed a drastic shift of phase boundaries.[84] A hybrid self-consistent field theory and liquid state integral equation theory (SCFT-LS) demonstrates that the ionically charged blocks of diblock copolymers significantly skew the phase boundaries toward a lower volume fraction of charged blocks.[65] The extent of boundary shift increases as a function of charge fraction and Coulombic interaction strengths. Similarly, dissipative particle dynamics (DPD) simulations show this shift of phase boundaries with an increasing charge fraction.[85] Further development of these theoretical approaches incorporating polarized field effects are needed to improve the understanding of phase behavior in precise ion-containing $(AB)_n$ multiblock copolymers.

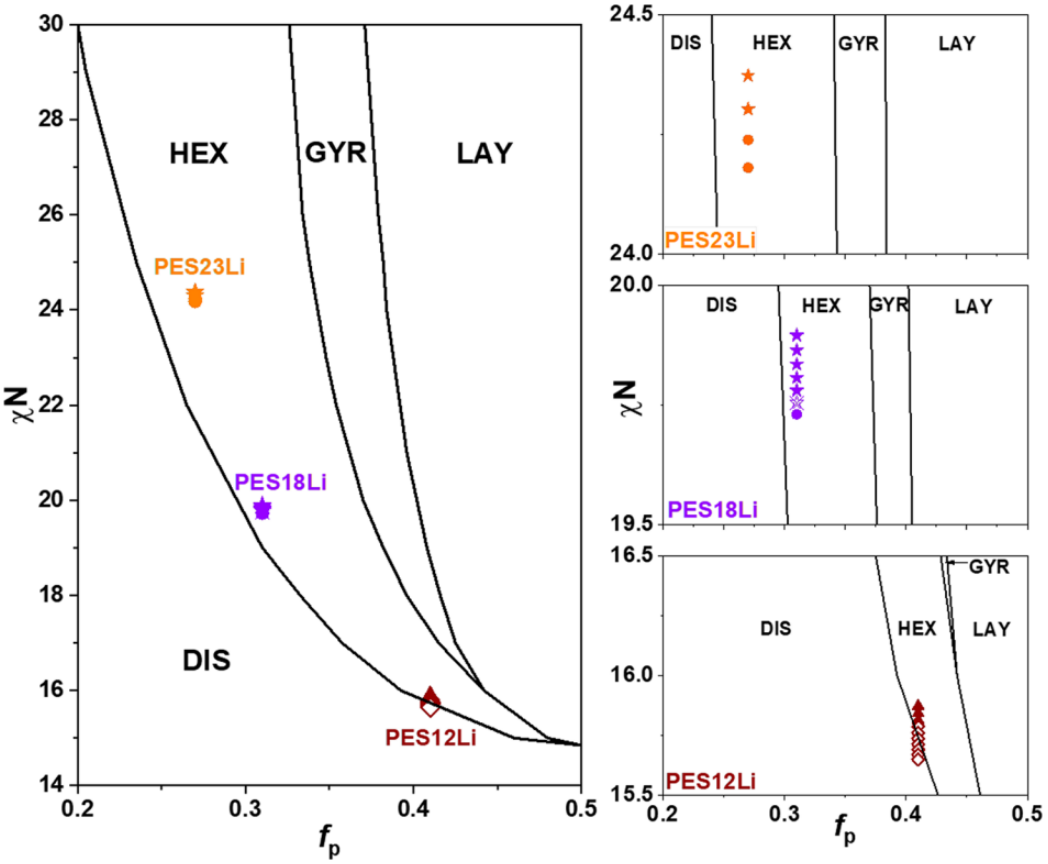

Figure 9. Experimentally observed morphologies (symbols) of PES*x*Li (x = 12, 18, 23) above T_m and numerically determined phase boundaries (lines) of $(AB)_{17}$ multiblock copolymers from SCFT calculations. Symbol shapes represent the morphologies of PES*x*Li: GYR (★), HEX (●), LAY (▲), and DIS (◇). The three plots at the right expand the χN scale for clarity of the experimental results. Reprinted from ref 62. Copyright 2021 American Chemical Society.

Double Gyroid Morphologies in Thin Films of PES18Li

To provide a deeper understanding of morphology characteristics of precise ion-containing multiblock copolymers in confined geometries, PES*x*Li thin films were prepared and examined with *in-situ* grazing-incidence X-ray scattering (**Figure 10**).[86] At 40 °C, distinct in-plane scattering peaks at $q_y \sim 1.5$ Å^{-1} indicate that the crystalline hydrocarbon blocks pack with an interchain distance of 0.4 nm and the chain axis vertically aligned relative to the substrate (**Figure 10a**). The out-of-plane scattering peaks along the q_z-axis indicate well-defined ionic layers parallel to the substrate, where the layer spacing is 3.1 nm (**Figure 10d**). Upon heating above T_m, the layered morphology spontaneously transitions into highly-oriented DG with an epitaxial transition from the (100) plane of LAY to the (211) plane of DG parallel to the substrate

(**Figure 10e**).[87] The domain spacing calculated from the primary (211) peak of the DG structure is ~2.5 nm. Further heating to 180 °C allows an epitaxial transition of DG into HEX morphology, where the cylinders are parallel to the substrate (**Figure 10f**).[19] The transitions between the DG and HEX are reversible, and the DG to LAY transition is kinetically trapped due to slow crystallization consistent with bulk behavior. The film thickness in **Figure 10** is 44 nm and corresponds to ~7 cubic lattices of the DG structure, ~7a_{DG}. The DG morphology also forms in 26-nm films (~4a_{DG}), although a thinner film of 17 nm (~2.5a_{DG}) leads to coexisting DG and HEX morphologies due to greater confinement. This thin-film study demonstrates the exceptional fidelity of precise ion-containing $(AB)_n$ multiblock copolymers for designing DG structures and other ordered morphologies in thin films, which could develop into a versatile platform of ion transport membranes, filtration membranes, and templates for pattern transfer.

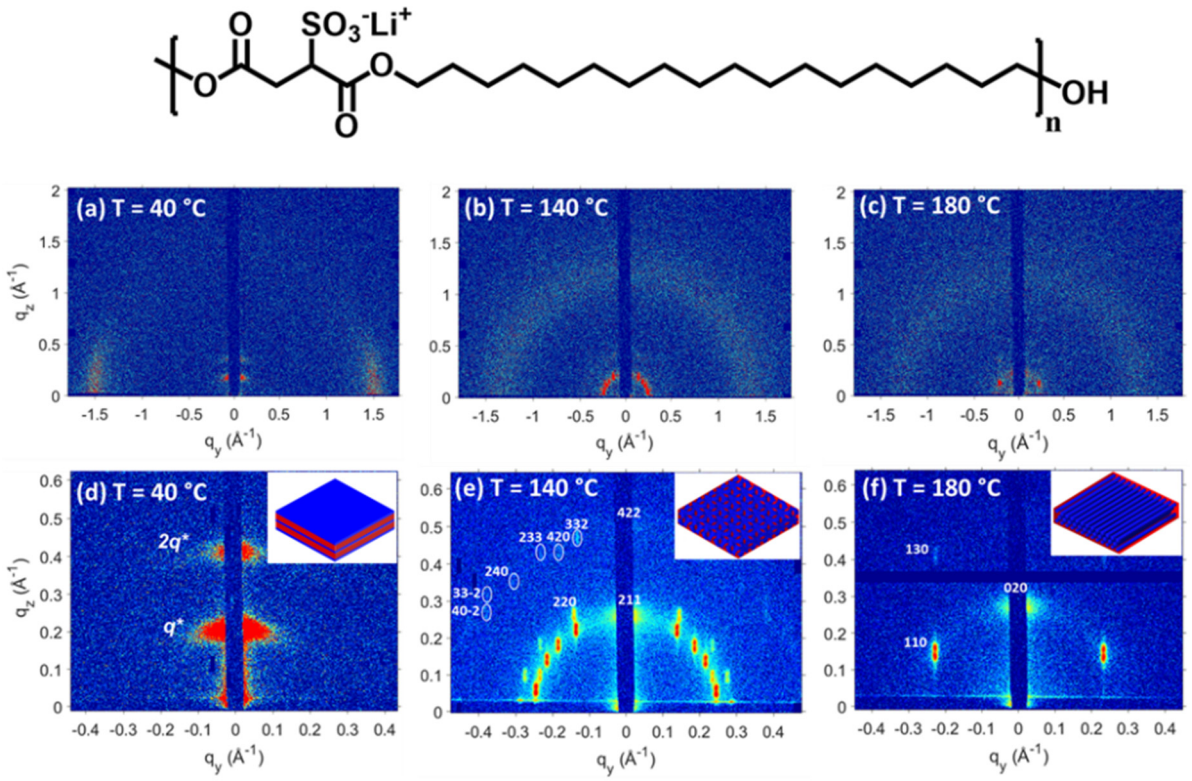

Figure 10. *In-situ* 2D grazing incidence (a-c) wide-angle and (d-f) small-angle X-ray scattering patterns of PES18Li thin films (~44 nm thick) at 40 °C, 140 °C, and 180 °C showing parallel layers, aligned double-gyroids, and parallel cylinders. Miller indexes in (e) and (f) are shown for the double-gyroid and 2D orthorhombic lattices, respectively. The incident angles were larger than the critical angle in these grazing incident measurements. Adapted from ref 86. Copyright 2022 American Chemical Society.

Criteria for Designing Double Gyroid in $(AB)_n$ Multiblock Copolymers

So far, this perspective has highlighted the DG morphology in one class of $(AB)_n$ multiblock copolymers composed of alternating polyester sulfonate with a metal counterion and hydrocarbon blocks. After inspecting results from other classes of $(AB)_n$ polymers, we will propose criteria for achieving the DG morphology. First, the removal of ionic groups from PES23M results in the absence of ordered morphologies above T_m, and we attribute this to a significant reduction in χ.[7] Therefore, the blocks of $(AB)_n$ multiblock copolymers should be highly incompatible to achieve ordered morphologies at sub 10-nm length scales.

Figure 11 shows a polyethylene oxide (PEO) based multiblock copolymer synthesized by the A_2 + B_2 melt polycondensation of a hydroxy-terminated oligo(ethylene glycol) monomer and a 5-sulfoisophthalate salt.[88] In these ionomers, PEO lengths of $m \sim 9$ and 13 with Li^+, Na^+, and Cs^+ exhibit disordered ionic aggregate morphologies with an amorphous PEO backbone. When the length of PEO is long enough at $m \sim 25$ and 75, the PEO blocks crystallize and the ionic aggregates form layers. Upon heating above the T_m, these PEO-based multiblock copolymers do not form ordered morphologies such as DG and HEX. The absence of ordered morphologies in these PEO-based ionomers can be attributed to the absence of precision in block lengths and the lack of chain flexibility in the polar block. First, the PEO block lengths are polydisperse as compared to the precise hydrocarbon lengths of the PES*x*M polymers. It is well-established that randomly distributed spacer lengths give rise to poorly defined ionic aggregate morphologies compared to precise spacer lengths.[89–91] Second, the polar blocks with rigid phenyl ring in the backbone are less flexible and impede the chain packing necessary to form DG or HEX morphologies. In addition, the segregation strength of these PEO-based ionomers will be weaker than polyethylene-based PES*x*M multiblock copolymers, pushing them toward the disordered state. The lack of precision in block length, a rigid polar block, and a smaller χ combine to impede the self-assembly of these PEO-based sodium sulfonated polyesters into ordered nanostructures.

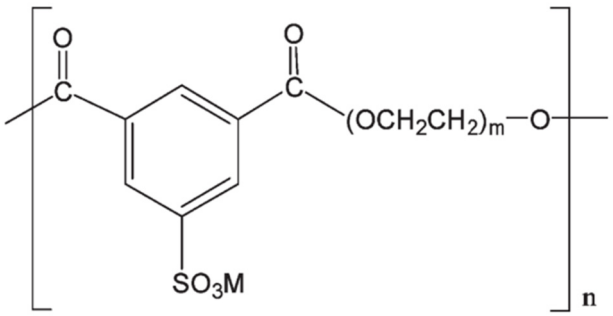

Figure 11. Poly(ethylene oxide)-based sulfonated polyesters with counterion (M) have poly(ethylene oxide) blocks of various average molecular weights: 400, 600, 1100, and 3300 g/mol correspond to $m \sim 9$, 13, 25, and 75 and $f_p = 0.31 - 0.05$. Reprinted from ref 88. Copyright 2010 American Chemical Society.

Figure 12a shows the precise acid-containing polymers synthesized via acyclic diene metathesis (ADMET) polymerization of diene monomers containing a symmetric pendant functionality. All-atom molecular dynamics simulations at $T > T_m$ show that the precise polymer containing COO^-Li^+ on every 21st carbon (p21AA-Li, $f_p = 0.15$) exhibits disordered, stringy, and percolated ionic aggregates, **Figure 12b**.[92] Similar stringy ionic aggregates are formed above T_m when the periodicity between the ionic groups is shorter (p9AA-Li and p15AA-Li),[92,93] indicating that the non-periodic packing of ionic aggregates is preferred relative to ordered morphologies in these ADMET polymers with pendant acid or ionic groups. One exception to this generalization is the precise ADMET polymer containing geminal phosphonic acids on exactly every 21st carbon (p21gPA, $f_p = 0.25$) that exhibits low symmetry diffraction peaks assigned to spherical aggregates on a face-centered cubic (FCC) lattice symmetry (**Figure 12c**).[94,95] In comparison with the PES*x*M polymers that contain ester linkages and short polar blocks, the ADMET polymers have all-carbon polymer backbones and the pendant groups on just one carbon. These features of the acid- and ion-containing ADMET polymers provide fewer chain conformations to accommodate microphase separation of the functional groups and prevent self-assembly into ordered morphologies, including the DG morphology. Given the chemical similarities between these ADMET polymers and the ionic lipids that originally displayed the DG morphology,[1] the absence of the DG in these polymers is unexpected.

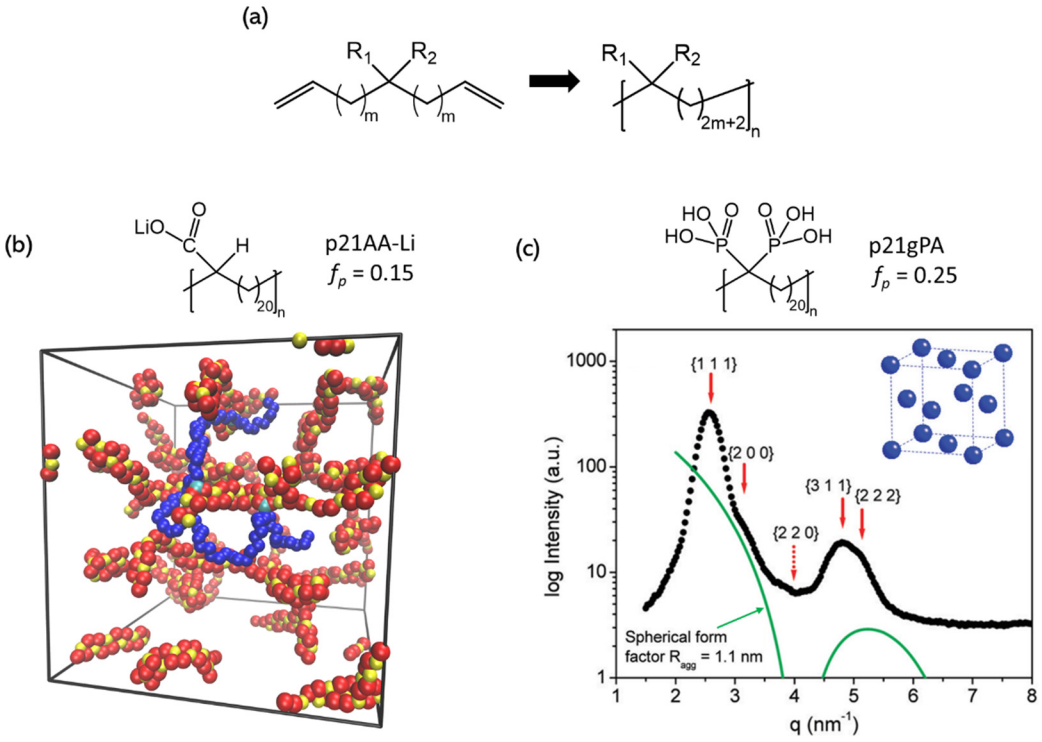

Figure 12. (a) ADMET polymerization to synthesize precise polymers. (b) Snapshot of precise polymers containing COO^-Li^+ on every 21st carbon (p21AA-Li) from all-atom molecular dynamics simulation at 600K. All oxygen (red) and lithium (yellow) atoms of COO^-Li^+ are shown. Carbon atoms of one polymer chain are shown in blue and cyan denotes the carbon atoms of COO^-Li^+ of the polymer chain. The carbons of other polymer chains and all hydrogens are not displayed for clarity. The box size is 6.1 nm. Adapted from ref 92. Copyright 2019 American Chemical Society. (c) X-ray scattering profile of precise polymers containing geminal phosphonic acid groups on every 21st carbon (p21gPA) at room temperature. Peak positions correspond to spherical acid aggregates on a FCC lattice. Adapted from ref 94. Copyright 2013 American Chemical Society.

The physicochemical properties of the ionic groups, chain flexibility, and block incompatibility of the PES*x*M polymers provide insight into designing DG-forming multiblock copolymers. Below we propose four criteria for $(AB)_n$ multiblock copolymers to produce the DG and other ordered morphologies at sub-10 nm length scales.

- The A and B blocks are highly incompatible, for example, pairing ionic and non-ionic blocks.
- Both the A and B blocks are comprised of flexible chains to accommodate the surface curvature of the double gyroid structure and other ordered morphologies.

- The lengths of the A and B blocks are precise so that the polydispersity index of the AB unit is exactly 1.00.
- The volume fraction of the minority block is 0.27 – 0.41 to form double gyroid structures. Lower and higher volume fraction can form hexagonally packed cylinders or layers, respectively.

Conclusion

This Perspective summarizes the recent developments of precise ion-containing multiblock copolymers that self-assemble into double-gyroid structures at an unusually wide composition range of > 14 vol%. Step-growth polymerization methods could be developed to synthesize an even wider variety of precise ion-containing multiblock copolymers, and greatly expand the investigation of self-assembly in $(AB)_n$ copolymers. Current self-consistent field theories fail to capture the phase behavior of these precise ion-containing polymers, and this is primarily attributed to the presence of charges that induce electrostatic interactions and significant density fluctuations. A combination of experimental, theoretical, and simulation studies are required to fully establish a foundation for designing ordered nanostructures including DG with precise ion-containing multiblock copolymers.

Numerous applications can be envisioned for new $(AB)_n$ multiblock copolymer synthesized by step-growth polymerization. First, precise multiblock copolymers could be used for nanopatterning templates to achieve sub-3 nm domain spacings by having ultrahigh-χ and low-N. Key next steps include exploring multiblock copolymer kinetics, directed self-assembly of ultrahigh-χ polymers, and sequential infiltration synthesis within sub-3 nm domains to improve etching contrast. In addition, porous materials templated from the precise multiblock copolymers could be explored as filtration membranes. Another set of potential applications involves selective ion transport, including single-ion conductors having covalently bonded ionic functionalities to the polymer backbone as in the PES*x*M polymers. The ordered morphologies in thin films of these ion-containing polymers create well-aligned ion transport channels, which can be further optimized for high ionic conductivity by selecting optimal block chemistries from step-growth

polymerization and by the selective solvation with additives to swell the polar domains and dissociate the ion pairs. Precise ion-containing multiblock copolymers have great potential to expand understanding of block copolymer physics and address a variety of technological challenges.

AUTHOR INFORMATION

Corresponding Author

Karen I. Winey − Department of Materials Science and Engineering, University of Pennsylvania, Philadelphia, Pennsylvania 19104, United States.

Department of Chemical and Biomolecular Engineering, University of Pennsylvania, Philadelphia, Pennsylvania 19104, United States

orcid.org/0000-0001-5856-3410; Email: winey@seas.upenn.edu

Author

Jinseok Park − Department of Materials Science and Engineering, University of Pennsylvania, Philadelphia, Pennsylvania 19104, United States; orcid.org/0000-0002-0389-9707

ACKNOWLEDGMENTS

J.P. and K.I.W. acknowledge funding by the NSF DMR (1904767). J.P. and K.I.W. are grateful to Amalie Frischknecht, Edwin Thomas, and Stefan Mecking for valuable discussions. Figure 12b was generously provided by A.F. from simulations performed in Ref 76.

References

(1) Luzzati, V.; Spegt, P. A. Polymorphism of Lipids. *Nature* **1967**, *215*, 701–704.

(2) Hajduk, D. A.; Harper, P. E.; Gruner, S. M.; Honeker, C. C.; Kim, G.; Fetters, L. J.; Kim, G. The Gyroid: A New Equilibrium Morphology in Weakly Segregated Diblock Copolymers. *Macromolecules* **1994**, *27*, 4063–4075.

(3) Pötschke, P.; Paul, D. R. Formation of Co-Continuous Structures in Melt-Mixed Immiscible Polymer Blends. *J. Macromol. Sci. - Polym. Rev.* **2003**, *43*, 87–141.

(4) Dair, B. J.; Honeker, C. C.; Alward, D. B.; Avgeropoulos, A.; Hadjichristidis, N.; Fetters, L. J.; Capel, M.; Thomas, E. L. Mechanical Properties and Deformation Behavior of the Double Gyroid Phase in Unoriented Thermoplastic Elastomers. *Macromolecules* **1999**, *32*, 8145–8152.

(5) Dair, B. J.; Avgeropoulos, A.; Hadjichristidis, N.; Thomas, E. L. Mechanical Properties of the Double Gyroid Phase in Oriented Thermoplastic Elastomers. *J. Mater. Sci.* **2000**, *35*, 5207–5213.

(6) Cho, B. K.; Jain, A.; Gruner, S. M.; Wiesner, U. Mesophase Structure-Mechanical and Ionic Transport Correlations in Extended Amphiphilic Dendrons. *Science (80-.).* **2004**, *305*, 1598–1601.

(7) Yan, L.; Rank, C.; Mecking, S.; Winey, K. I. Gyroid and Other Ordered Morphologies in Single-Ion Conducting Polymers and Their Impact on Ion Conductivity. *J. Am. Chem. Soc.* **2020**, *142*, 857–866.

(8) Jo, G.; Ahn, H.; Park, M. J. Simple Route for Tuning the Morphology and Conductivity of Polymer Electrolytes: One End Functional Group Is Enough. *ACS Macro Lett.* **2013**, *2*, 990–995.

(9) Ichikawa, T.; Yoshio, M.; Hamasaki, A.; Mukai, T.; Ohno, H.; Kato, T. Self-Organization of Room-Temperature Ionic Liquids Exhibiting Liquid-Crystalline Bicontinuous Cubic Phases: Formation of Nano-Ion Channel Networks. *J. Am. Chem. Soc.* **2007**, *129*, 10662–10663.

(10) Dolan, J. A.; Wilts, B. D.; Vignolini, S.; Baumberg, J. J.; Steiner, U.; Wilkinson, T. D. Optical Properties of Gyroid Structured Materials: From Photonic Crystals to Metamaterials. *Adv. Opt. Mater.* **2015**, *3*, 12–32.

(11) Hur, K.; Francescato, Y.; Giannini, V.; Maier, S. A.; Hennig, R. G.; Wiesner, U. Three-Dimensionally Isotropic Negative Refractive Index Materials from Block Copolymer Self-Assembled Chiral Gyroid Networks. *Angew. Chemie - Int. Ed.* **2011**, *50*, 11985–11989.

(12) Feng, X.; Zhuo, M.; Guo, H.; Thomas, E. L. Visualizing the Double-Gyroid Twin. *Proc. Natl. Acad. Sci. U. S. A.* **2021**, *118*, 1–6.

(13) Wang, H. F.; Chiu, P. T.; Yang, C. Y.; Xie, Z. H.; Hung, Y. C.; Lee, J. Y.; Tsai, J. C.; Prasad, I.; Jinnai, H.; Thomas, E. L.; Ho, R. M. Networks with Controlled Chirality via Self-Assembly of Chiral Triblock Terpolymers. *Sci. Adv.* **2020**, *6*.

(14) Thomas, E. L.; Alward, D. B.; Kinning, D. J.; Martin, D. C.; Handlin, D. L.; Fetters, L. J. Ordered

Bicontinuous Double-Diamond Structure of Star Block Copolymers: A New Equilibrium Microdomain Morphology. *Macromolecules* **1986**, *19*, 2197–2202.

(15) Winey, K. I.; Gobran, D. A.; Zhongde, X.; Fetters, L. J.; Thomas, E. L. Compositional Dependence of the Order-Disorder Transition in Diblock Copolymers. *Macromolecules* **1994**, *27*, 2392–2397.

(16) Förster, S.; Khandpur, A. K.; Zhao, J.; Bates, F. S.; Hamley, I. W.; Ryan, A. J.; Bras, W. Complex Phase Behavior of Polyisoprene-Polystyrene Diblock Copolymers Near the Order-Disorder Transition. *Macromolecules* **1994**, *27*, 6922–6935.

(17) Khandpur, A. K.; Förster, S.; Bates, F. S.; Hamley, I. W.; Ryan, A. J.; Bras, W.; Almdal, K.; Mortensen, K. Polyisoprene-Polystyrene Diblock Copolymer Phase Diagram near the Order-Disorder Transition. *Macromolecules* **1995**, *28*, 8796–8806.

(18) Hajduk, D. A.; Harper, P. E.; Gruner, S. M.; Honeker, C. C.; Thomas, E. L.; Fetters, L. J. A Reevaluation of Bicontinuous Cubic Phases in Starblock Copolymers. *Macromolecules* **1995**, *28*, 2570–2573.

(19) Schulz, M. F.; Bates, F. S. Epitaxial Relationship for Hexagonal-to-Cubic Phase Transition in a Block Copolymer Mixture. *Phys. Rev. Lett.* **1994**, *73*, 86–89.

(20) Schulz, M. F.; Khandpur, A. K.; Bates, F. S.; Almdal, K.; Mortensen, K.; Hajduk, D. A.; Gruner, S. M. Phase Behavior of Polystyrene-Poly(2-Vinylpyridine) Diblock Copolymers. *Macromolecules* **1996**, *29*, 2857–2867.

(21) Zhao, J.; Majumdar, B.; Schulz, M. F.; Bates, F. S.; Almdal, K.; Mortensen, K.; Hajduk, D. A.; Gruner, S. M. Phase Behavior of Pure Diblocks and Binary Diblock Blends of Poly(Ethylene)-Poly(Ethylethylene). *Macromolecules* **1996**, *29*, 1204–1215.

(22) Bates, F. S.; Schulz, M. F.; Khandpur, A. K.; Förster, S.; Rosedale, J. H.; Almdal, K.; Mortensen, K. Fluctuations, Conformational Asymmetry and Block Copolymer Phase Behaviour. *Faraday Discuss.* **1994**, *98*, 7–18.

(23) Castelletto, V.; Hamley, I. W. Morphologies of Block Copolymer Melts. *Curr. Opin. Solid State Mater. Sci.* **2004**, *8*, 426–438.

(24) Meuler, A. J.; Hillmyer, M. A.; Bates, F. S. Ordered Network Mesostructures in Block Polymer Materials. *Macromolecules* **2009**, *42*, 7221–7250.

(25) Cochran, E. W.; Garcia-Cervera, C. J.; Fredrickson, G. H. Stability of the Gyroid Phase in Diblock Copolymers at Strong Segregation. *Macromolecules* **2006**, *39*, 2449–2451.

(26) Matsen, M. W.; Bates, F. S. Unifying Weak- and Strong-Segregation Block Copolymer Theories. *Macromolecules* **1996**, *29*, 1091–1098.

(27) Matsen, M. W.; Bates, F. S. Block Copolymer Microstructures in the Intermediate-Segregation Regime. *J. Chem. Phys.* **1997**, *106*, 2436–2448.

(28) Davidock, D. A.; Hillmyer, M. A.; Lodge, T. P. Persistence of the Gyroid Morphology at Strong Segregation in Diblock Copolymers. *Macromolecules* **2003**, *36*, 4682–4685.

(29) Wohlgemuth, M.; Yufa, N.; Hoffman, J.; Thomas, E. L. Triply Periodic Bicontinuous Cubic Microdomain Morphologies by Symmetries. *Macromolecules* **2001**, *34*, 6083–6089.

(30) Reddy, A.; Feng, X.; Thomas, E. L.; Grason, G. M. Block Copolymers beneath the Surface: Measuring and Modeling Complex Morphology at the Subdomain Scale. *Macromolecules* **2021**, *54*, 9223–9257.

(31) Matsen, M. W. Effect of Architecture on the Phase Behavior of AB-Type Block Copolymer Melts. *Macromolecules* **2012**, *45*, 2161–2165.

(32) Winey, K. I.; Thomas, E. L.; Fetters, L. J. Ordered Morphologies in Binary Blends of Diblock Copolymer and Homopolymer and Characterization of Their Intermaterial Dividing Surfaces. *J. Chem. Phys.* **1991**, *95*, 9367–9375.

(33) Winey, K. I.; Thomas, E. L.; Fetters, L. J. Isothermal Morphology Diagrams for Binary Blends of Diblock Copolymer and Homopolymer. *Macromolecules* **1992**, *25*, 2645–2650.

(34) Sakurai, S.; Umeda, H.; Furukawa, C.; Irie, H.; Nomura, S.; Lee, H. H.; Kim, J. K. Thermally Induced Morphological Transition from Lamella to Gyroid in a Binary Blend of Diblock Copolymers. *J. Chem. Phys.* **1998**, *108*, 4333–4339.

(35) Roy, R.; Park, J. K.; Young, W. S.; Mastroianni, S. E.; Tureau, M. S.; Epps, T. H. Double-Gyroid Network Morphology in Tapered Diblock Copolymers. *Macromolecules* **2011**, *44*, 3910–3915.

(36) Avgeropoulos, A.; Dair, B. J.; Hadjichristidis, N.; Thomas, E. L. Tricontinuous Double Gyroid Cubic Phase in Triblock Copolymers of the ABA Type. *Macromolecules* **1997**, *30*, 5634–5642.

(37) Kossuth, M. B.; Morse, D. C.; Bates, F. S. Viscoelastic Behavior of Cubic Phases in Block Copolymer Melts. *J. Rheol. (N. Y. N. Y).* **1999**, *43*, 167–196.

(38) Sakurai, S.; Isobe, D.; Okamoto, S.; Nomura, S. Control of Mechanical Properties via Morphological Control through Blending of Elastomeric Polystyrene-Block-Polybutadiene-Block-Polystyrene Triblock Copolymers. *Mater. Sci. Res. Int.* **2001**, *7*, 225–228.

(39) Shefelbine, T. A.; Vigild, M. E.; Matsen, M. W.; Hajduk, D. A.; Hillmyer, M. A.; Cussler, E. L.; Bates, F. S. Core-Shell Gyroid Morphology in a Poly(Isoprene-Block-Styrene-Block-Dimethylsiloxane) Triblock Copolymer. *J. Am. Chem. Soc.* **1999**, *121*, 8457–8465.

(40) Bailey, T. S.; Pham, H. D.; Bates, F. S. Morphological Behavior Bridging the Symmetric AB and ABC States in the Poly(Styrene-b-Isoprene-b-Ethylene Oxide) Triblock Copolymer System. *Macromolecules* **2001**, *34*, 6994–7008.

(41) Epps, T. H.; Cochran, E. W.; Bailey, T. S.; Waletzko, R. S.; Hardy, C. M.; Bates, F. S. Ordered Network Phases in Linear Poly(Isoprene-b-Styrene-b-Ethylene Oxide) Triblock Copolymers.

Macromolecules **2004**, *37*, 8325–8341.

(42) Chatterjee, J.; Jain, S.; Bates, F. S. Comprehensive Phase Behavior of Poly(Isoprene-b-Styrene-b-Ethylene Oxide) Triblock Copolymers. *Macromolecules* **2007**, *40*, 2882–2896.

(43) Matsushita, Y.; Torikai, N.; Suzuki, J.; Seki, M. Interfacial Structures of Triblock Copolymers and Their Chain Conformations in Bulk. *J. Phys. Chem. Solids* **1999**, *60*, 1279–1284.

(44) Seki, M.; Suzuki, J.; Matsushita, Y. Small-Angle X-Ray Scattering Analysis of the Periodic Tricontinuous Network Structure of Symmetric ABC Triblock Copolymers. *J. Appl. Crystallogr.* **2000**, *33*, 285–290.

(45) Suzuki, J.; Seki, M.; Matsushita, Y. The Tricontinuous Double-Gyroid Structure from a Three-Component Polymer System. *J. Chem. Phys.* **2000**, *112*, 4862–4868.

(46) Winey, K. I.; Thomas, E. L.; Fetters, L. J. The Ordered Bicontinuous Double-Diamond Morphology in Diblock Copolymer/Homopolymer Blends. *Macromolecules* **1992**, *25*, 422–428.

(47) Matsen, M. W. Phase Behavior of Block Copolymer/Homopolymer Blends. *Macromolecules* **1995**, *28*, 5765–5773.

(48) Lai, C. T.; Shi, A. C. Binary Blends of Diblock Copolymers: An Effective Route to Novel Bicontinuous Phases. *Macromol. Theory Simulations* **2021**, *30*, 1–9.

(49) Yu, B.; Li, R.; Segalman, R. A. Tuning the Double Gyroid Phase Window in Block Copolymers via Polymer Chain Conformation near the Interface. *Macromolecules* **2021**, *54*, 5388–5396.

(50) Floudas, G.; Vazaiou, B.; Schipper, F.; Ulrich, R.; Wiesner, U.; Iatrou, H.; Hadjichristidis, N. Poly(Ethylene Oxide-b-Isoprene) Diblock Copolymer Phase Diagram. *Macromolecules* **2001**, *34*, 2947–2957.

(51) Leibler, L.; Benoit, H. Theory of Correlations in Partly Labelled Homopolymer Melts. *Polymer (Guildf).* **1981**, *22*, 195–201.

(52) Burger, C.; Ruland, W.; Semenov, A. N. Polydispersity Effects on the Microphase-Separation Transition in Block Copolymers. *Macromolecules* **1990**, *23*, 3339–3346.

(53) Lynd, N. A.; Hillmyer, M. A. Influence of Polydispersity on the Self-Assembly of Diblock Copolymers. *Macromolecules* **2005**, *38*, 8803–8810.

(54) Lynd, N. A.; Meuler, A. J.; Hillmyer, M. A. Polydispersity and Block Copolymer Self-Assembly. *Prog. Polym. Sci.* **2008**, *33*, 875–893.

(55) Li, Y.; Qian, H. J.; Lu, Z. Y.; Shi, A. C. Enhancing Composition Window of Bicontinuous Structures by Designed Polydispersity Distribution of ABA Triblock Copolymers. *Polymer (Guildf).* **2013**, *54*, 6253–6260.

(56) Widin, J. M.; Schmitt, A. K.; Im, K.; Schmitt, A. L.; Mahanthappa, M. K. Polydispersity-Induced Stabilization of a Disordered Bicontinuous Morphology in ABA Triblock Copolymers.

Macromolecules **2010**, *43*, 7913–7915.

(57) Widin, J. M.; Schmitt, A. K.; Schmitt, A. L.; Im, K.; Mahanthappa, M. K. Unexpected Consequences of Block Polydispersity on the Self-Assembly of ABA Triblock Copolymers. *J. Am. Chem. Soc.* **2012**, *134*, 3834–3844.

(58) Meuler, A. J.; Ellison, C. J.; Hillmyer, M. A.; Bates, F. S. Polydispersity-Induced Stabilization of the Core-Shell Gyroid. **2008**, 6272–6275.

(59) Bates, F. S.; Hillmyer, M. a.; Lodge, T. P.; Bates, C. M.; Delaney, K. T.; Fredrickson, G. H. Multiblock Polymers: Panacea or Pandora's Box? *Science (80-.).* **2012**, *336*, 434–440.

(60) Benoit, H.; Hadziioannou, G. Scattering Theory and Properties of Block Copolymers with Various Architectures in the Homogeneous Bulk State. *Macromolecules* **1988**, *21*, 1449–1464.

(61) Li, S.; Xu, Q.; Li, K.; Yu, C.; Zhou, Y. High-χ Alternating Copolymers for Accessing Sub-5 Nm Domains via Simulations. *Phys. Chem. Chem. Phys.* **2020**, *22*, 5577–5583.

(62) Park, J.; Staiger, A.; Mecking, S.; Winey, K. I. Sub-3-Nanometer Domain Spacings of Ultrahigh-χ Multiblock Copolymers with Pendant Ionic Groups. *ACS Nano* **2021**, *15*, 16738–16747.

(63) Smith, S. D.; Spontak, R. J.; Satkowski, M. M.; Ashraf, A.; Heape, A. K.; Lin, J. S. Microphase-Separated Poly(Styrene-b-Isoprene)n Multiblock Copolymers with Constant Block Lengths. *Polymer (Guildf).* **1994**, *35*, 4527–4536.

(64) Wu, L.; Cochran, E. W.; Lodge, T. P.; Bates, F. S. Consequences of Block Number on the Order-Disorder Transition and Viscoelastic Properties of Linear (AB)n Multiblock Copolymers. *Macromolecules* **2004**, *37*, 3360–3368.

(65) Sing, C. E.; Zwanikken, J. W.; Olvera De La Cruz, M. Electrostatic Control of Block Copolymer Morphology. *Nat. Mater.* **2014**, *13*, 694–698.

(66) Park, J.; Staiger, A.; Mecking, S.; Winey, K. I. Structure-Property Relationships in Single-Ion Conducting Multiblock Copolymers: A Phase Diagram and Ionic Conductivities. *Macromolecules* **2021**, *54*, 4269–4279.

(67) Park, M. J.; Balsara, N. P. Phase Behavior of Symmetric Sulfonated Block Copolymers. *Macromolecules* **2008**, *41*, 3678–3687.

(68) Shim, J.; Bates, F. S.; Lodge, T. P. Superlattice by Charged Block Copolymer Self-Assembly. *Nat. Commun.* **2019**, *10*, 1–7.

(69) Min, J.; Jung, H. Y.; Jeong, S.; Lee, B.; Son, C. Y.; Park, M. J. Enhancing Ion Transport in Charged Block Copolymers by Stabilizing Low Symmetry Morphology: Electrostatic Control of Interfaces. *Proc. Natl. Acad. Sci. U. S. A.* **2021**, *118*, 1–8.

(70) Ruzette, A.-V. G.; Soo, P. P.; Sadoway, D. R.; Mayes, A. M. Melt-Formable Block Copolymer Electrolytes for Lithium Rechargeable Batteries. *J. Electrochem. Soc.* **2001**, *148*, A537.

(71) Wanakule, N. S.; Virgili, J. M.; Teran, A. A.; Wang, Z. G.; Balsara, N. P. Thermodynamic Properties of Block Copolymer Electrolytes Containing Imidazolium and Lithium Salts. *Macromolecules* **2010**, *43*, 8282–8289.

(72) Nakamura, I.; Balsara, N. P.; Wang, Z. G. Thermodynamics of Ion-Containing Polymer Blends and Block Copolymers. *Phys. Rev. Lett.* **2011**, *107*, 1–5.

(73) Teran, A. A.; Balsara, N. P. Thermodynamics of Block Copolymers with and without Salt. *J. Phys. Chem. B* **2014**, *118*, 4–17.

(74) Thelen, J. L.; Teran, A. A.; Wang, X.; Garetz, B. A.; Nakamura, I.; Wang, Z. G.; Balsara, N. P. Phase Behavior of a Block Copolymer/Salt Mixture through the Order-to-Disorder Transition. *Macromolecules* **2014**, *47*, 2666–2673.

(75) Loo, W. S.; Galluzzo, M. D.; Li, X.; Maslyn, J. A.; Oh, H. J.; Mongcopa, K. I.; Zhu, C.; Wang, A. A.; Wang, X.; Garetz, B. A.; Balsara, N. P. Phase Behavior of Mixtures of Block Copolymers and a Lithium Salt. *J. Phys. Chem. B* **2018**, *122*, 8065–8074.

(76) Mayes, A M; Olvera De La Cruz, M. Equilibrium Domain Spacing in Weakly Segregated Block Copolymers. *Macromolecules* **1991**, *24*, 3975–3976.

(77) Hadziioannou, G.; Skoulios, A.; Hadziioannou, G. Molecular Weight Dependence of Lamellar Structure in Styrene/Isoprene Two- and Three-Block Copolymers. *Macromolecules* **1982**, *15*, 258–262.

(78) Almdal, K.; Rosedale, J. H.; Bates, F. S.; Wignall, G. D.; Fredrickson, G. H. Gaussian- to Stretched-Coil Transition in Block Copolymer Melts. *Phys. Rev. Lett.* **1990**, *65*, 1112–1115.

(79) Foster, M. D.; Sikka, M.; Singh, N.; Bates, F. S.; Satija, S. K.; Majkrzak, C. F. Structure of Symmetric Polyolefin Block Copolymer Thin Films. *J. Chem. Phys.* **1992**, *96*, 8605–8615.

(80) Yue, Z.; Sivaniah, E.; Hashimoto, T. SAXS Analysis of the Order-Disorder Transition and the Interaction Parameter of Polystyrene-Block-PoIy(Methyl Methacrylate). *Macromolecules* **2008**, *41*, 9948–9951.

(81) Sinturel, C.; Bates, F. S.; Hillmyer, M. A. High χ-Low N Block Polymers: How Far Can We Go? *ACS Macro Lett.* **2015**, *4*, 1044–1050.

(82) Grzetic, D. J.; Delaney, K. T.; Fredrickson, G. H. The Effective χ Parameter in Polarizable Polymeric Systems: One-Loop Perturbation Theory and Field-Theoretic Simulations. *J. Chem. Phys.* **2018**, *148*, 204903.

(83) Grzetic, D. J.; Delaney, K. T.; Fredrickson, G. H. Field-Theoretic Study of Salt-Induced Order and Disorder in a Polarizable Diblock Copolymer. *ACS Macro Lett.* **2019**, *8*, 962–967.

(84) Grzetic, D. J.; Delaney, K. T.; Fredrickson, G. H. Electrostatic Manipulation of Phase Behavior in Immiscible Charged Polymer Blends. *Macromolecules* **2021**, *54*, 2604–2616.

(85) Zhai, C.; Zhou, H.; Gao, T.; Zhao, L.; Lin, S. Electrostatically Tuned Microdomain Morphology and Phase-Dependent Ion Transport Anisotropy in Single-Ion Conducting Block Copolyelectrolytes. *Macromolecules* **2018**, *51*, 4471–4483.

(86) Park, J.; Staiger, A.; Mecking, S.; Winey, K. I. Ordered Nanostructures in Thin Films of Precise Ion-Containing Multiblock Copolymers. *ACS Cent. Sci.* **2022**, *8*, 388–393.

(87) Hajduk, D. A.; Ho, R. M.; Hillmyer, M. A.; Bates, F. S.; Almdal, K. Transition Mechanisms for Complex Ordered Phases in Block Copolymer Melts. *J. Phys. Chem. B* **1998**, *102*, 1356–1363.

(88) Wang, W.; Liu, W.; Tudryn, G. J.; Colby, R. H.; Winey, K. I. Multi-Length Scale Morphology of Poly(Ethylene Oxide)-Based Sulfonate Ionomers with Alkali Cations at Room Temperature. *Macromolecules* **2010**, *43*, 4223–4229.

(89) Seitz, M. E.; Chan, C. D.; Opper, K. L.; Baughman, T. W.; Wagener, K. B.; Winey, K. I. Nanoscale Morphology in Precisely Sequenced Poly(Ethylene-Co-Acrylic Acid) Zinc Ionomers. *J. Am. Chem. Soc.* **2010**, *132*, 8165–8174.

(90) Hall, L. M.; Seitz, M. E.; Winey, K. I.; Opper, K. L.; Wagener, K. B.; Stevens, M. J.; Frischknecht, A. L. Ionic Aggregate Structure in Ionomer Melts: Effect of Molecular Architecture on Aggregates and the Ionomer Peak. *J. Am. Chem. Soc.* **2012**, *134*, 574–587.

(91) Trigg, E. B.; Tiegs, B. J.; Coates, G. W.; Winey, K. I. High Morphological Order in a Nearly Precise Acid-Containing Polymer and Ionomer. *ACS Macro Lett.* **2017**, *6*, 947–951.

(92) Frischknecht, A. L.; Paren, B. A.; Middleton, L. R.; Koski, J. P.; Tarver, J. D.; Tyagi, M.; Soles, C. L.; Winey, K. I. Chain and Ion Dynamics in Precise Polyethylene Ionomers. *Macromolecules* **2019**, *52*, 7939–7950.

(93) Frischknecht, A. L.; Winey, K. I. The Evolution of Acidic and Ionic Aggregates in Ionomers during Microsecond Simulations. *J. Chem. Phys.* **2019**, *150*, 064901.

(94) Buitrago, C. F.; Opper, K. L.; Wagener, K. B.; Winey, K. I. Precise Acid Copolymer Exhibits a Face-Centered Cubic Structure. *ACS Macro Lett.* **2012**, *1*, 71–74.

(95) Buitrago, C. F.; Jenkins, J. E.; Opper, K. L.; Aitken, B. S.; Wagener, K. B.; Alam, T. M.; Winey, K. I. Room Temperature Morphologies of Precise Acid-and Ion-Containing Polyethylenes. *Macromolecules* **2013**, *46*, 9003–9012.

TOC Graphic